# Dual Planar-Helix Type Energy Storage Wires to Circumvent Universal Energy Lag Effect

*Inho Nam, Jongseok Park, Soomin Park, Seongjun Bae, Young Geun Yoo, and Jongheop Yi**

Wire-shaped energy storage systems have become cutting edge technology in the energy-science field within the past decade.[1,2] Such energy systems are taking center stage for application to postmodern electronics and related multidisciplinary fields such as fashion and culture.[3–5] Until now, the mainstream direction in modern electronics (and energy storage) including flexibility, wearability, and implantability have involved the use of conventional planar systems.[6,7] However, the 2D structure of the conventional formats has hindered their development in terms of performance and moldability.[2] In view of mechanics, plane structures in 2D essentially have a unidirectional folding characteristics. On the other hand, wires with 1D structure have an omnidirectional serpentine structure in the other axes. Compared with 2D planar formats, wire types can be easily integrated into unique structures such as variety of textiles that can be used in our daily life.[2–5]

Although 1D structures can be strong, challenges fundamentally remain in the use of wire-type energy storage. In conventional energy storage, energy is simply improved, either by increasing the specific energy of materials or widening the operational voltage range.[8,9] However, wire-type energy storage still have a low energy density even in cases of the systems that include cutting edge materials in energy-science field, such as high-surface carbon allotropes for improving electrical double layer (EDL) charge and inorganic compounds, or conducting polymers inducing faradaic reaction.[10–18] From the standpoint of physics, such a bottleneck is reasonable because the current technologies associated with energy storage wires do not satisfy the theoretical assumptions of electromagnetism that have been in use for the past several decades. For example, in an ordinary charged plane, the electric field is assumed to be uniform and to have a 1D direction. On the other hand, the electrodes in wire-type energy storage have a cylindrical structure which actually causes a 2D and decaying electric field.[19] In spite of the analytical problem, the exact potential distribution and performance model for wire-type energy storage, including a double-helix structure have not been exploited until now. A theoretical analysis is one of most important aspects for the sustainable development of the energy storage field in next generation.

Here, we propose two possibilities regarding energy storage wires, especially, wire-type supercapacitors. (1) We investigated the electrochemical performance of universal wire-type supercapacitor using an analytical derivation. From the derived equations, we verified that a difference exists between wire-type and conventional planar supercapacitors and identified the fundamental limits of wire-type supercapacitors. We refer to this limit as an "energy lag effect." (2) To exclude the identified limits, we designed a supercapacitor thread having completely different structure compared with previous wire-type energy storage systems. The supercapacitor thread was designed as a dual plane-helix structure and does not show performance limits, experimentally and analytically. Finally, the structure was applied to a flexible textile and an integrated parallel and series circuit analogous to show its structural advantage compared to a conventional wire types with cylindrical electrodes. In here, we only focused on a capacitive energy storage because most wire-type energy storage was realized as the form of supercapacitors. The unique properties of the capacitive energy storage include a fast charge/discharge capacity, long life cycle, wide range of operating temperatures, and safety, suggesting that they are higher applicable for use in next multidisciplinary devices than conventional batteries.[20–22] However, the strategy proposed here can be extended to other cylindrical electrodes that are currently used in wire-type lithium ion batteries.

From electromagnetism, a charged plane creates 1D and uniform electric fields: $E = Q/\varepsilon_0 A$, where E is the electric field, $Q$ is the total charge on the charged plane, $\varepsilon_0$ is the permittivity of free space, and A is the vector area of the plane (Figure S1a, Supporting Information). With this equation, it is possible to assume that an ordinary planar electrode also has a homogeneous E with the exception of edge effects. On the other hand, a wire-type electrode has a cylindrical structure. Therefore, it makes E in a radial direction, and the E is inversely proportional along with a radial vector, r. The calculated E in a wire structure via Gauss's law is derived as an Equation (1) with Figure S1b in the Supporting Information

$$E = \frac{Q}{\varepsilon_0 2\pi r L} \tag{1}$$

The difference in E causes a disparity in the charged energy in the electrodes. The "energy lag effect" is defined as the energy density gap between a planar and cylindrical electrode constituting wire-type energy storage. To be specific, we analytically derived an equation for the difference of capacitance densities ($C_{sp}$) in planar and wire-type supercapacitors.

I. Nam, J. Park, S. Park, S. Bae, Y. G. Yoo, Prof. J. Yi
WCU Program of Chemical Convergence for Energy and Environment
School of Chemical and Biological Engineering
Institute of Chemical Processes
Seoul National University
Seoul 151-742, Republic of Korea
E-mail: jyi@snu.ac.kr

DOI: 10.1002/aenm.201501812

  

In the supercapacitor or an EDL capacitor system, the volume between two electrodes is filled with an electrolyte. Therefore, an electrical potential ($\psi$) is generated in the system between the surface of the electrode and attractive counter ions in the electrolyte. In conclusion, considering the different structures, plane and wire, it is possible to simultaneously create different EDL models on each electrode in this charge situation.

The sophisticated picture of a conventional planar EDL has been described using the Gouy–Chapman–Stern (GCS) model during the past decades.[23] The GCS model is derived from the combination of the von Helmholtz and Gouy–Chapman model using a Poisson–Boltzmann (P–B) equation with a Cartesian coordinate. Regardless of the coordinate system, the P–B equation is governed by a differential form as follows[24]

$$\nabla^2\psi = \frac{-\rho}{\varepsilon_r\varepsilon_0} \text{ and}$$
$$\rho = e\left[z_+c_{\infty+}\exp\left(\frac{-z_+e\psi}{k_BT}\right) - z_-c_{\infty-}\exp\left(\frac{z_-e\psi}{k_BT}\right)\right] \quad (2)$$

From Equation (2), the differential form of a $\psi$ in EDL can be described in Equation (3) with a valence of electrolyte

$$(\varepsilon_r\varepsilon_0\nabla\psi) = \begin{cases} 0 & \text{in Stern layer} \\ 2ezC_\infty \sinh\left(\frac{ze\psi}{k_BT}\right) & \text{in diffuse layer} \end{cases} \quad (3)$$

where $\rho$ is the charge per unit volume, $\varepsilon_r$ is the dielectric constant of the solvent, $e$ the electron charge, $z$ the ionic charge, $c_\infty$ the bulk ion concentration, $k_B$ the Boltzmann constant, and $T$ the absolute temperature. At low ion concentration, the P–B equation was already solved on a cylindrical coordinate using a numerical method for applications in plasma physics or DNA double-helix structure mixed with liposomes.[25,26] In a supercapacitor system, a simple Stern layer (or a Helmholtz layer) can be used as depicted EDL without a diffuse layer, because it is reasonable for a relatively high ion concentration where a diffuse layer is not expected to play a major role analogous to the schematics in **Figure 1**a,b.[27,28] The assumption is well operated in a variety of supercapacitor electrolytes, e.g., 1 M $H_3PO_4$ and 6 M KOH in aqueous solvent or 1.5 M tetraethylammonium tetrafluoroborate in nonaqueous solvent ($TEABF_4$/$CH_3CN$).[29,30] In this context, the P–B equation is simplified as a Laplace's equation ($\nabla^2\psi = 0$) in supercapacitor systems. The Laplace's equation expresses $\psi$ related to one electrode in a supercapacitor system. However, $\Delta\psi$ is almost zero in a bulk electrolyte and the $\psi$ has an inverse symmetry on both electrodes, therefore the equation can show the distribution of $\psi$ for the entire system. In Figure S2 in the Supporting Information, we showed the relationship between $\psi$ and the dimensionless location of electrodes in planar and cylindrical supercapacitors. In conclusion, it is possible to analytically solve the differential equation and to understand the electrochemical performance of a wire-type supercapacitor.

The capacitances ($C$) of planar and wire-type supercapacitors are depicted as in Equations (4) and (5) with Figure S3 in the Supporting Information. $C$ can be determined by the relations; $C \equiv Q/\Delta\psi$. The $\Delta\psi$ is calculated by the integration of Laplace's equation that arises from Equation (3) with a Cartesian and cylindrical coordinate, respectively. The boundary conditions of the calculation are that if $t = t_0$ and $r = r_0$, $Q$ = constant in the surface of the electrode. $t_0$ is the half-thickness of the electrode, $r_0$ is the radius of the electrode, and $Q$ is a total charge on the charged surface

$$C \equiv \frac{Q}{\Delta\psi} = \frac{\varepsilon_r\varepsilon_0 A}{t - t_0} \quad (4)$$
if $t = t_0$, $Q$ = constant in a planar electrode

$$C \equiv \frac{Q}{\Delta\psi} = \frac{2\pi\varepsilon_r\varepsilon_0 L}{\ln(r/r_0)} \quad (5)$$
if $r = r_0$, $Q$ = constant in a cylindrical electrode

Equation (5) is similar to an EDL model in the cylindrical pore structure of carbon as previously researched.[27,29] In consequence, the capacitance densities ($C_{sp}$) in planar and wire-type electrodes are as follows

$$C_{sp} \equiv \frac{C}{v} = \frac{\varepsilon_r\varepsilon_0}{t_0(t - t_0)} \quad \text{in planar electrode} \quad (6)$$

$$C_{sp} \equiv \frac{C}{v} = \frac{2\varepsilon_r\varepsilon_0}{r_0^2\ln(r/r_0)} \quad \text{in cylindrical electrode} \quad (7)$$

where $v$ is the volume of electrode. Equations (6) and (7) prove that a $C_{sp}$ and energy density is closely related to the morphology of the electrode. According to the following Equation (8), it is reasonable that the wire-type supercapacitors would have a lower capacitance compared to that of 2D planar supercapacitors made up of identical materials

$$\Delta C_{sp} \equiv C_{sp\ plane} - C_{sp\ wire} = 2\varepsilon_r\varepsilon_0\left(\frac{1}{2t_0(t - t_0)} - \frac{1}{r_0^2\ln(r/r_0)}\right) \quad (8)$$

We refer to the $\Delta C_{sp}$ between planar and cylindrical electrodes as the energy lag effect in supercapacitor or capacitance lag effect. In Figure 1, the distance between surface of electrode and counter ions ($d$) is uniform and it is same with a radii of solvated counter ions. Therefore, $d = t - t_0 = r - r_0$ in Figure S3 in the Supporting Information. If $d \ll r$, $r_0\ln(r/r_0) \cong r - r_0$.[28,30] Most reported wire-type supercapacitor systems satisfy this assumption, therefore the capacitance lag effect is simplified as Equation (9).[10–18]

$$\Delta C_{sp} = \frac{2\varepsilon_r\varepsilon_0}{d}\left(\frac{1}{2t_0} - \frac{1}{r_0}\right) \quad (9)$$

The calculated ratio of $C_{sp\ plane}/C_{sp\ wire}$ using the capacitance lag model (Equation (9) is $r_0/2t_0$. This result is independent of the absolute radii in wire electrodes because specific shapes cannot influence the absolute volume of identical materials. To make $C_{sp\ plane}/C_{sp\ wire}$ to be under 1, the ratio of width and thickness ($a/2t_0$ in Figure S3 in the Supporting Information) in

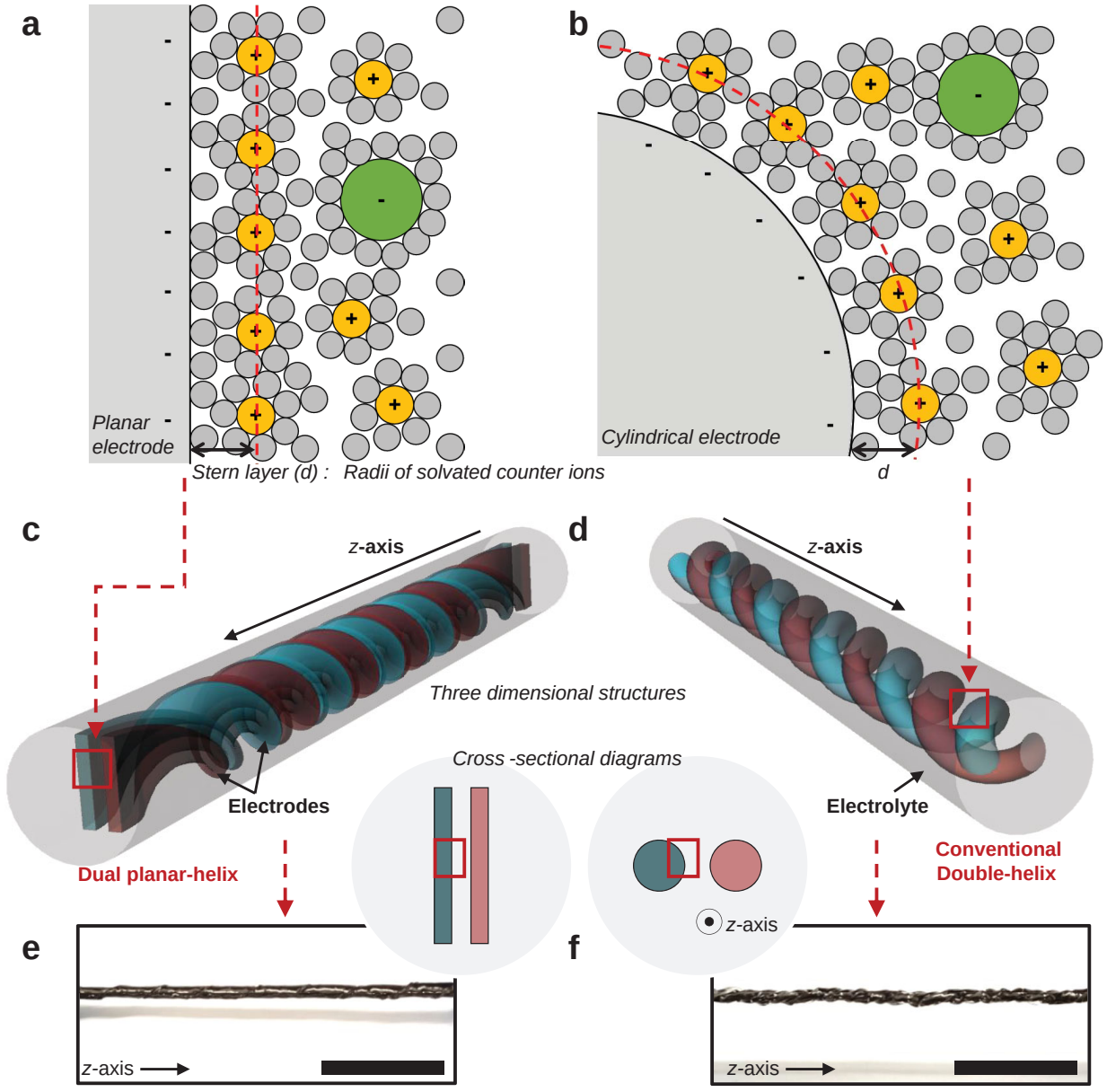


**Figure 1.** Schematics of an EDL on a planar electrode and a cylindrical electrode. The sophisticated pictures of EDL on a) planar electrode and b) cylindrical electrode. Schematics of c) dual planar-helix and d) double helix wire-type supercapacitors. Optical images of e) dual planar-helix and f) double helix wire-type supercapacitors. The scale bars are 10 mm in length.

plane electrodes must be under $\pi$ (≈3.14). In practice, the ratio in plane electrodes is at least >10, therefore $r_0 \gg 2t_0$. In conclusion, conventionally shaped supercapacitor wires always have a lower energy density than 2D planar supercapacitors regardless of absolute size when identical materials are used. From the analytic interpretations and schemes, we can not only prove the fundamental limitation of wire types, but also find a breakthrough to circumvent this geological issue.

In order to solve the capacitance lag effect, supercapacitor wires must not have conventional double-helix structures. We proposed a new design of a supercapacitor wire that contains a dual planar-helix structure (Figure 1c–f). In the systems, parallel and elongated flat electrodes are located at opposite sites and twisted together, and both electrodes are separated by a gel-polymer electrolyte (GPE). The twisting is a way to construct wire-type supercapacitors utilizing elongated planar electrodes. The way of twisting for the elongated planar supercapacitor was presented in Figure S4 in the Supporting Information. In this helix structure, the *z*-axis is symmetrical without considering edge effects. By the symmetry and a superposition law, the electrochemical properties of the supercapacitor are consistent along with *z*-axis. In conclusion, the dual planar-helix type supercapacitor has a complete wire structure and the performance is analytically the same as an ordinary 2D planar supercapacitor,

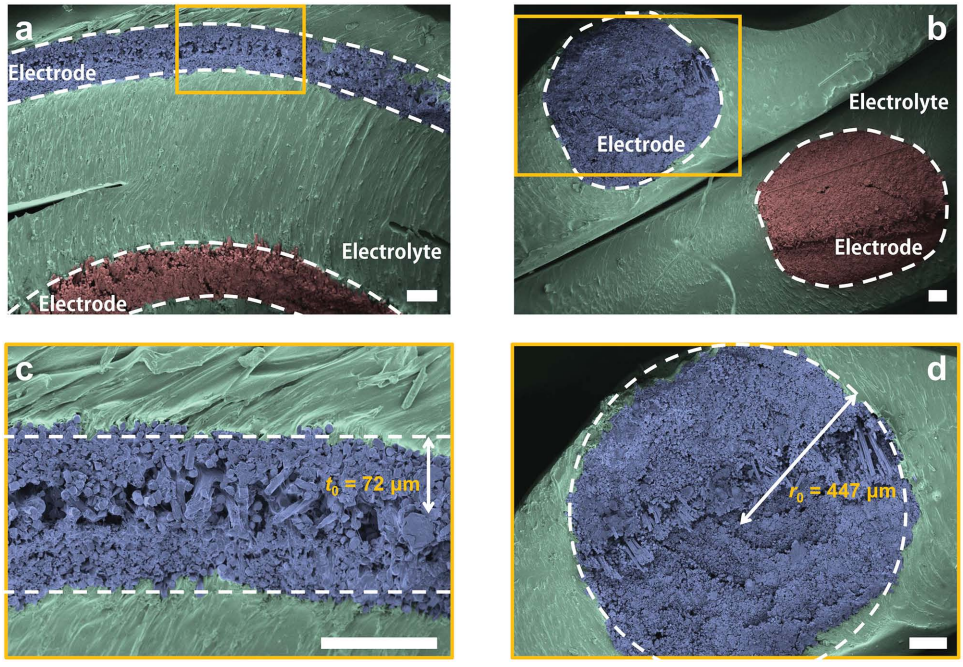


**Figure 2.** Structure difference of dual planar-helix and double helix wire-type supercapacitors. Scanning electron microscope cross-sectional images of a,c) dual planar-helix and b,d) double helix wire-type supercapacitors. c,d) High-resolution images. The scale bars are 100 μm in length.

which means that the dual planar-helix types do not show the energy lag effect observed in universal wire-type energy storage.

The proof-of-concept experiments for the planar-helix structure are based on a commercial carbon wires as an electrode and PVA/$H_3PO_4$ as a GPE (**Figure 2**). Carbon allotropes were well known members of supercapacitor electrodes,[31,32] and PVA/$H_3PO_4$ GPE is widely used due to its nontoxic nature and possible coupling of charge transport.[33,34] The GPE in the system serves as a separator, glue, electrolyte, and elastic skeleton component at once. The dual planar-helix supercapacitor wires do not require the additional loading of active materials or post treatment to increase their performance, which is another distinct advantage of this system over conventional wire-type supercapacitors from an engineering view point. The selected materials for the electrode and GPE are replaceable and are not limited in the system.

For a control experiment, we fabricated both dual planar-helix and conventional double-helix supercapacitor wires using identical electrodes and electrolyte. The morphologies of the fabricated supercapacitors can be seen clearly in optical and scanning electron microscopic (SEM) images (Figures 1e,f and 2). The electrical resistances of the electrodes were measured as shown in Figure S5 in the Supporting Information. The resistances of electrodes with a planar and a cylindrical shape are 3.03 and 2.94 Ω, respectively. Both electrodes showed equivalent values of resistances, which represents that the difference in the performance of two systems is determined by geometry, not conductivity. These results of electrical conductivity are rational, because the material (carbon wire) and the length (8 cm) of electrodes of both dual planar-helix and double-helix type supercapacitors used are identical. The electrochemical properties and the resistive behavior of the planar-helix and double-helix systems were examined by cyclic voltammetry (CV) and galvanostatic charge/discharge (C–D) analyzes shown in **Figure 3**a,b, respectively. The prototype device with planar-helix structure has a 3.14 F $cm^{-3}$ of $C_{sp}$ at a current density of 4 mA $cm^{-3}$ and the value is converted as 19.72 mF $cm^{-1}$ of capacitance per unit length of the wire (see calculation details in Supporting Information). This value is about from three times to two orders of magnitude higher than that of currently available 1D electrodes, such as carbon fibers (0.504 mF $cm^{-1}$) and carbon nanotubes (CNTs) (0.51 mF $cm^{-1}$) in EDL capacitors,[12,13] $MnO_2$/CNT (0.022 mF $cm^{-1}$) and $Ni(OH)_2$/ordered mesoporous carbon (6.67 mF $cm^{-1}$) as transition metal oxides,[14,15] polyaniline/CNT as a conducting polymer electrode (0.9 mF $cm^{-1}$) in pseudocapacitor,[16] respectively. In addition, it is further possible to increase the performance of the conceptual system by using cutting edge electrode materials similar to conventional wire types, e.g., metal oxide hybrids for inducing pseudocapacitance behavior.

The $C_{sp}$ of dual planar-helix supercapacitor (1.91 F $cm^{-3}$ at 10 mV $s^{-1}$) is 3.0 times higher than that of a double-helix type prepared using the identical materials (0.66 F $cm^{-3}$ at 10 mV $s^{-1}$). The calculated ratio of $C_{sp\ dual\ planar\text{-}helix}/C_{sp\ double\text{-}helix}$ using the capacitance lag model (the ratio = $r_0/2t_0$) is 3.36 which is similar to the measured ratio (≈3) from experiments. This proves that the analytical model describing the energy lag effects operates well and is rationally applicable to real systems. When the scan rate was increased from 3 to 50 mV $s^{-1}$, approximately 30% of its original capacitance was measured (Figure 3a). The $C_{sp}$ values were found to be 2.59, 2.30, 1.91, 1.45, 1.16, and 0.76 F $cm^{-3}$ for scan rates of 3, 5, 10, 20, 30, and 50 mV $s^{-1}$, respectively. Although the system exhibited a slight resistive behavior at a scan rate of 50 mV $s^{-1}$, the measured CVs

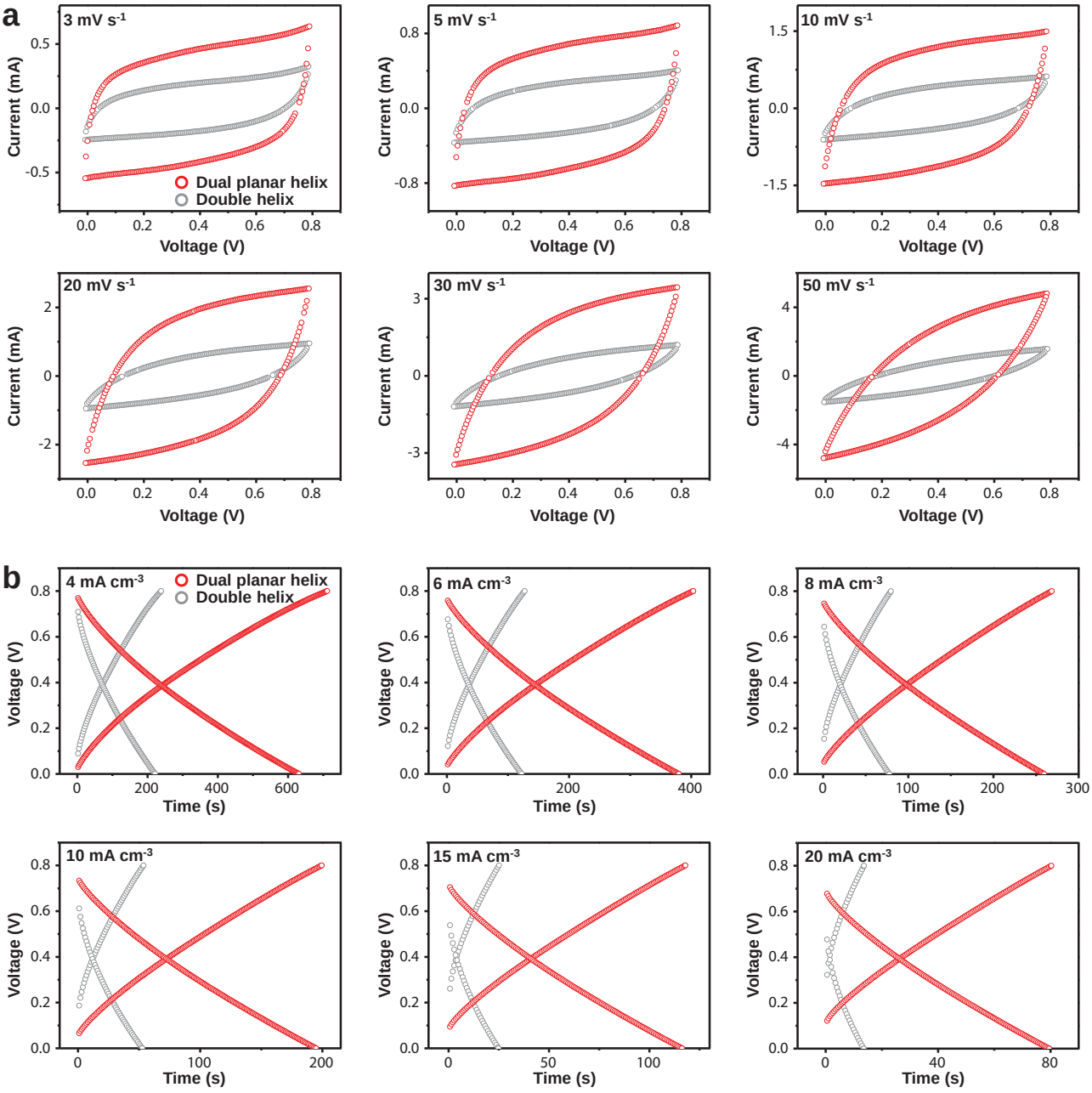


**Figure 3.** Electrochemical properties of dual planar-helix and double helix wire-type supercapacitors. a) Cyclic voltammograms of dual planar-helix and double helix wire-type supercapacitors at various scan rates (3, 5, 10, 20, 30, and 50 mV $s^{-1}$). b) Galvanostatic charge–discharge profiles of dual planar-helix and double helix wire-type supercapacitors at various current densities (4, 6, 8, 10, 15, and 20 mA $cm^{-3}$).

retained a reasonable rectangular shape.[35] From C–D analyzes, the planar-helix type obviously exhibited a longer discharge time than that values based on the double-helix structure. With planar-helix electrodes, $C_{sp}$ values of 3.14, 2.84, 2.59, 2.43, 2.17, and 1.98 F $cm^{-3}$ were achieved at various current densities of 4, 6, 8, 10, 15, and 20 mA $cm^{-3}$, respectively. Whereas, the double-helix type only showed $C_{sp}$ of 1.10, 0.91, 0.77, 0.66, 0.46, and 0.34 mF $cm^{-3}$ at same current densities (Figure 3b). All of the above electrochemical results not only prove the correctness of the energy lag effect but also show the advantage of dual planar-helix types in view of performance. The stability of a supercapacitor is also an important parameter for evaluating the suitability of systems for practical applications. Figure S6 in the Supporting Information shows the cycling stability of the planar-type during a repetitive C–D analysis. The structure showed good cyclic stability, and it maintained a capacitance of over 90% of the original value at the initial cycle even after 10 000 charge–discharge cycles. For control experiments, the electrochemical performances of the dual planar-helix wire-type supercapacitor before and after twisting were evaluated.

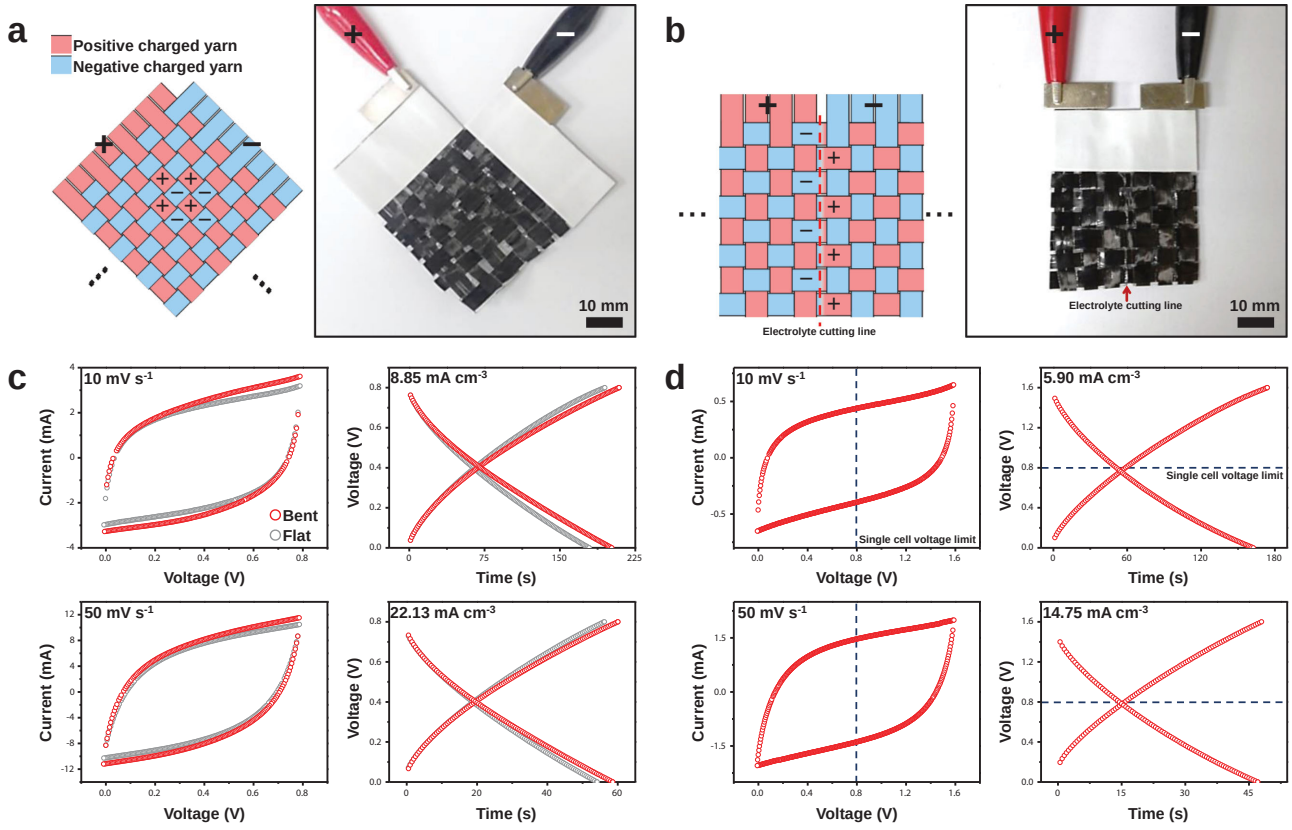


**Figure 4.** Woven textile composite with warp and weft electrodes. Schematics of $n \times n$ warps or wefts connected in a) parallel and b) series and optics images of woven textile composited with $6 \times 6$ warps or wefts. In the schematics, the red lines and blue lines show positive and negative charged yarns, respectively. In (b), center line appears location of cutting line of sectionalized electrolyte. Cyclic voltammograms and charge/discharge curves of the textile supercapacitor with c) parallel and d) series circuit analogs. In (c), the red dots indicate the characteristic in bending deformation and the gray dots show that in flat. The blue lines in (d) show the stable potential window (0.8 V) of single supercapacitor wires.

As shown in Figure S7 in the Supporting Information, the cyclic voltammetry curves of the supercapacitor before and after twisting were identical, which means that the electrochemical performances are equal irrespective of the twisting deformation.

Concerning the applicability of such systems in wearable devices, many wire-type energy storage have been incorporated into textile products.[17,18] In a further study, we applied our planar threads as warp and weft yarns themselves and used them to prepare textiles as shown in **Figure 4**. The planar-type carbon thread was first capsulated with GPE, and was then used as a warp or weft. The yarns were in intimate contact, thus guaranteeing a good ion-transport pathway the same as the planar-type supercapacitor. In the energy storage cloth, the extension is easily permitted with parallel and series connections. Figure 4a,b illustrates the schematics of $n \times n$ warps or wefts connected in parallel and series (wire length is 36 mm). From CV and C–D analyzes, the output current of parallel connected textiles were increased by a factor of three compared with the single planar-helix supercapacitor wire (Figure 4c). We also evaluated the electrochemical characteristics of the textile under severe bending conditions. There was actually a small increase (about 10%) in capacitance when the systems are bent (the curvature, $k$, is 4 $cm^{-1}$ and bending radius is 2.5 mm). The improved performance can be attributed to the fact that the bending condition induces pressure in orthogonal direction between GPEs and electrodes as observed in our previous studies.[6,36] This also suggests that there is no significant change in the carbon thread electrode when the supercapacitor was in a severely bent shape, which is in good agreement with the 3D finite elemental modeling (3D-FEM) of the carbon thread in Figure S8 (see details in the Supporting Information). In Figure 4d, an enhanced voltage range with the combination of series connection is also provided. In conclusion, the current and voltage range can be easily improved by connecting the wires in parallel or in series analogs to meet the power and energy demands needed. The electrochemical properties are maintained at various rates regardless of the type of circuits and deformation conditions as proved by a series of CV and C–D analyzes (Figures S9 and S10 in the Supporting Information).

Here, we addressed two sequential topics that are of interest for universal wire-type supercapacitors. First, we analytically designed a valid method for calculating the cutting edge wire-type supercapacitor based on fundamental electromagnetism. Second, we fabricated rationally optimized supercapacitor threads based on this knowledge. The fabricated high performance supercapacitor could be transformed into wires, textile, and integrated parallel and series circuit

analogous. We believe that our concept has important implications across a number of disciplines that are directed toward the development of next generation energy storage and multidisciplinary electronics.

## Experimental Section

*Fabrication of Planar and Cylindrical Shape Elongated Electrodes*: Commercial carbon wires (Taekwang Co.) were used as an electrode for fabricating the supercapacitor wire. The commercial carbon wires have an elongated planar structure and are composed of microsized carbon fibers and sizing agents to maintain the planar structure.[37] The sizing agent was eliminated by heat and acid treatments before changing the structure. To eliminate the organic sizing agent (epoxy resin) on the surface, the electrode was heated under an $N_2$ flow at 800 °C (2 h), followed by an additional acidic treatment (12 h) using the mixture of sulfuric acid (95 wt%) and nitric acid (60 wt%) in 3:1 (v/v). The acid-treated carbon thread was rinsed with deionized water followed by a complete drying at 60 °C in an oven. The elimination of sizing agent was verified by X-ray photoelectron spectroscopy analyzes (XPS) (Figure S8, Supporting Information). After the elimination of sizing agents, the planar structure can be converted to cylindrical shape by the agglomeration of carbon fibers in water. For the comparison of planar and cylindrical wire structures, the carbon fibers were shaped into planar structures (4.35 mm in width and 144 μm in depth) and cylindrical structures (447 μm of radius) (structural details are shown in Figure 2). The effective radii of dual planar-helix and double-helix type supercapacitor devices are 1.19 and 1.12 mm, respectively.

*Fabrication of Dual Planar-Helix and Double-Helix Type Supercapacitor Wires*: PVA/$H_3PO_4$ gel was used as a GPE. 5 g of PVA (Sigma, reagent grade, degree of polymerization: 2000–3000) was mixed with 40 mL deionized water and 2.4 mL of H3PO4 (85 wt%). The temperature was then raised to 358 K on a hot plate with sufficient stirring until a transparent gel was formed. This viscous liquid was poured onto the planar glass bath and allowed to spread to an equal thickness after a minute. As-synthesized carbon wires were placed in the PVA/$H_3PO_4$ gel solution for 12 h to complete the solidification. The other side of the wires was coated in the same way. Finally, the PVA-coated carbon thread electrodes (independent half-cells) were peeled off from the glass bath, combined in pairs by the graft force originated by the GPE and twisted to create a wire-type full cell.

*Weaving of Energy Storage Textiles with Warp and Weft Electrodes*: To fabricate textile supercapacitors with parallel circuit analogs, PVA-coated planar thread electrodes were placed together so as to cross over and under each other to produce a fabric with a checkered pattern (Figure 4a). In this study, a total of 12 electrodes were used in single textile supercapacitor cell, six in each direction. An additional step was needed to prepare series circuit analogs (Figure 4b). In the middle of the six electrodes laid on the same direction, there were uncoated GPE lines, one on each single thread. The sectionalized GPE line was fabricated by a lift off method which has been described in our previous research.[6] As a consequence, each side of textile sectionalized by GPE acted as an independent capacitor unit allowing the entire textile to be two supercapacitors in series.

*Characterization and Electrochemical Measurement*: Cross-sectional SEM images of dual planar-helix and double-helix wire-type supercapacitors were obtained using a field-emission scanning electron microscope operating at 2 kV with an in-lens detector (Sigma, Carl Zeiss). CV was carried out using a computer-controlled potentiostat (Zive sp2, Zive Lab) at various potential windows (0–1.6 V) and galvanostatic C–D) measurements were carried out using the same equipment at various current densities (4 –22.13 mA $cm^{-3}$). XPS spectra were obtained using a Kratos AXIS-HIS electron spectrometer equipped with a Mg–Ka X-ray source and a hemispherical electron energy analyzer.

## Supporting Information

Supporting Information is available from the Wiley Online Library or from the author.

## Acknowledgements

I.N. and J.P. contributed equally to this work. This research was supported by the Global Frontier R&D Program on Center for Multiscale Energy System funded by the National Research Foundation under the Ministry of Science, ICT & Future, Korea (Grant No. NRF-2011-0031571).

Received: September 10, 2015
Revised: October 28, 2015
Published online: December 3, 2015

[1] Y. Qin, X. Wang, Z. L. Wang, *Nature* **2008**, *451*, 809.
[2] S. Pan, Z. Zhang, W. Weng, H. Lin, Z. Yang, H. Peng, *Mater. Today* **2014**, *17*, 276.
[3] M. Hamedi, R. Forchheimer, O. Inganäs, *Nat. Mater.* **2007**, *6*, 357.
[4] Cutecircuit, www.cutecircuit.com, (accessed: 19, November 2015)
[5] Drumpants, www.drumpants.com, (accessed: 19, November 2015)
[6] J. A. Rogers, T. Someya, Y. Huang, *Science* **2010**, *327*, 1603.
[7] D.-H. Kim, N. Lu, R. Ma, Y.-S. Kim, R.-H. Kim, S. Wang, J. Wu, S. M. Won, H. Tao, A. Islam, K. J. Yu, T. Kim, R. Chowdhury, M. Ying, L. Xu, M. Li, H.-J. Chung, H. Keum, M. McCormick, P. Liu, Y.-W. Zhang, F. G. Omenetto, Y. Huang, T. Coleman, J. A. Rogers, *Science* **2011**, *333*, 838.
[8] P. Simon, Y. Gogotsi, *Nat. Mater.* **2008**, *7*, 845.
[9] I. Nam, G.-P. Kim, S. Park, J. Han, J. Yi, *Energy Environ. Sci.* **2014**, *7*, 1095.
[10] J. Bae, M. K. Song, Y. J. Park, J. M. Kim, M. Liu, Z. L. Wang, *Angew. Chem. Int. Ed.* **2011**, *50*, 1683.
[11] T. Chen, R. Hao, H. Peng, L. Dai, *Angew. Chem. Int. Ed.* **2015**, *54*, 618.
[12] Y. Fu, X. Cai, H. Wu, Z. Lv, S. Hou, M. Peng, X. Yu, D. Zou, *Adv. Mater.* **2012**, *24*, 5713.
[13] Y. Zhang, W. Bai, X. Cheng, J. Ren, W. Weng, P. Chen, X. Fang, Z. Zhang, H. Peng, *Angew. Chem. Int. Ed.* **2014**, *53*, 14564.
[14] J. Ren, L. Li, C. Chen, X. Chen, Z. Cai, L. Qiu, Y. Wang, X. Zhu, H. Peng, *Adv. Mater.* **2013**, *25*, 1155.
[15] X. Dong, Z. Guo, Y. Song, M. Hou, J. Wang, Y. Wang, Y. Xia, *Adv. Funct. Mater.* **2014**, *24*, 3405.
[16] Z. Zhang, J. Deng, X. Li, Z. Yang, S. He, X. Chen, G. Guan, J. Ren, H. Peng, *Adv. Mater.* **2015**, *27*, 356.
[17] J. A. Lee, M. K. Shin, S. H. Kim, H. U. Cho, G. M. Spinks, G. G. Wallace, M. D. Lima, X. Lepro, M. E. Kozlov, R. H. Baughman, S. J. Kim, *Nat. Commun.* **2013**, *4*, 1970.
[18] L. Kou, T. Huang, B. Zheng, Y. Han, X. Zhao, K. Gopalsamy, H. Sun, C. Gao, *Nat. Commun.* **2014**, *5*, 3754.
[19] D. J. Griffiths, *Introduction to Electrodynamics*, 4th ed., Addison-Wesley, Boston, MA, USA **2013**.
[20] J. Chmiola, C. Largeot, P.-L. Taberna, P. Simon, Y. Gogotsi, *Science* **2010**, *328*, 480.
[21] P. Yang, W. Mai, *Nano Energy* **2014**, *8*, 274.
[22] P. Simon, Y. Gogotsi, B. Dunn, *Science* **2014**, *343*, 1210.
[23] J. J. Lyklema, *Fundamentals of Interface and Colloid Science Volume II: Solid–Liquid Interfaces*, Academic Press, San Diego, CA, USA **1995**.
[24] J. Huang, R. Qiao, B. G. Sumpter, V. Meunier, *J. Mater. Res.* **2010**, *25*, 1469.
[25] D. Harries, *Langmuir* **1998**, *14*, 3149.
[26] I. A. Shkel, O. V. Tsodikov, M. T. Record Jr., *Proc. Natl. Acad. Sci. USA* **2002**, *99*, 2597.

  

[27] J. Huang, B. G. Sumpter, V. Meunier, *Angew. Chem. Int. Ed.* **2008**, *47*, 520.
[28] J. Chmiola, G. Yushin, Y. Gogotsi, C. Portet, P. Simon, P. L. Taberna, *Science* **2006**, *313*, 1760.
[29] J. Huang, B. G. Sumpter, V. Meunier, *Chem. Eur. J.* **2008**, *14*, 6614.
[30] J. Chmiola, C. Largeot, P.-L. Taberna, P. Simon, Y. Gogotsi, *Angew. Chem. Int. Ed.* **2008**, *47*, 3392.
[31] L. G. H. Staafn, P. Lundgren, P. Enoksson, *Nano Energy* **2014**, *9*, 128.
[32] G. Wang, L. Zhang, J. Zhang, *Chem. Soc. Rev.* **2012**, *41*, 797.
[33] M. Z. Kufian, S. R. Majid, A. K. Arof, *Ionics* **2007**, *13*, 231.
[34] N. A. Choudhury, S. Sampathb, A. K. Shukla, *Energy Environ. Sci.* **2009**, *2*, 55.
[35] E. Frackowiak, F. Beguin, *Carbon* **2001**, *39*, 937.
[36] I. Nam, S. Park, G.-P. Kim, J. Park, J. Yi, *Chem. Sci.* **2013**, *4*, 1663.
[37] Taekwang Industrial, Carbon fiber, www.taekwang.co.kr/en/product/product_4.asp, (accessed: 19, November 2015)